35th Annual International Conference of the IEEE EMBS
Osaka, Japan, 3 - 7 July, 2013

Validation of a multi-scale model of the coronary circulation in adult sheep and newborn lambs

Jonathan P. Mynard, Daniel J. Penny and Joseph J. Smolich

***Abstract*— We validated a multi-scale model of a left-dominant coronary circulation using high fidelity pressure and flow data acquired in adult sheep and newborn lambs. The model incorporated a one-dimensional representation of the major left conduit coronary arteries, allowing for the study of wave propagation effects. The coronary microvasculature was represented by regional instances of a lumped parameter model consisting of three transmural layers, each with two serial compartments accounting for compliance, resistance and intramyocardial pressure effects. Model inputs comprised measured aortic pressure/flow and ventricular pressure. Minimal data fitting was employed, with only measured mean coronary flow used to iteratively adjust total coronary resistance. The model was adapted to different heart sizes via allometric scaling. Excellent agreement was observed between model and experimental flow waveforms in the proximal circumflex artery, both in terms of the degree of systolic flow impediment and transient waveform features. The proposed multi-scale modelling approach is likely to be useful for studying phasic features of the coronary flow waveform, including coronary waves in different coronary anatomies and throughout development.**

I. INTRODUCTION

Many of the lumped parameter models used in the past to study mechanisms underlying the coronary flow waveform have focused primarily on the interplay between aortic pressure, coronary microvascular impedance and intramyocardial pressure, and therefore have not represented the large conduit coronary arteries in any detailed fashion [1], [2]. Recently, interest in the study of waves in conduit coronary arteries has been increasing [3]–[5], although the importance of wave propagation effects on flow waveforms is disputed [6], [7] and is hypothesized to vary during development due to changes in body size [8].

Multi-scale modelling is a promising avenue for studying both wave propagation effects and other phenomena crucial to coronary haemodynamics [7], however very little in-vivo validation of such models has been performed. Accordingly, in this study we propose a convenient and physiologically-relevant multi-scale modelling approach in which a one-dimensional (1D) representation of conduit coronary arteries is combined with a lumped parameter (0D) model of the coronary microvasculature. The multi-scale model is validated against high fidelity in-vivo measurements from adult sheep and newborn lambs, with allometric scaling used to adapt anatomical data from adult human studies [9].

J.P. Mynard, D.J. Penny and J.J. Smolich are with the Heart Research Group, Murdoch Childrens Research Institute and the Department of Paediatrics, University of Melbourne, Flemington Rd, Parkville, VIC 3052, Australia
jonathan.mynard@mcri.edu.au

II. METHODS

A. One-dimensional model of conduit arteries

Most sheep [10] and approximately 20% of humans [9] display a left dominant anatomy in which the posterior portion of the ventricular septum is supplied by distal branches of the circumflex coronary artery. Based on the gross similarity between left dominant anatomies in humans and sheep, branch anatomy (Fig. 1), segment lengths and diameters for the 1D conduit artery model were derived from measurements in humans [9], with specific values chosen to avoid non-physiological wave reflections at junctions.

Material properties of the 1D segments were imposed via a reference wave speed (c_0), calculated as a function of reference radius (r_0) using the empirical formula

$$c_0^2 = \frac{2}{3\rho}\left[k_1 \exp(k_2 r_0) + k_3\right] \tag{1}$$

Values for the coefficients k_1, k_2 and k_3 were taken from [11] and then all wave speed values were uniformly scaled to achieve a target value in the proximal circumflex coronary artery, where in-vivo data was acquired. The standard non-linear 1D equations governing pressure, velocity and cross-sectional area were solved as in [12], with a power law for the pressure-area relation [13],

$$p - p_{\text{ext}} = \frac{2\rho c_0^2}{b}\left[\left(\frac{A}{A_0}\right)^{b/2} - 1\right] + p_0 \tag{2}$$

where ρ is blood density (assumed value: 1.06 g/cm^3), A_0 and p_0 are reference area and pressure, and b was calculated

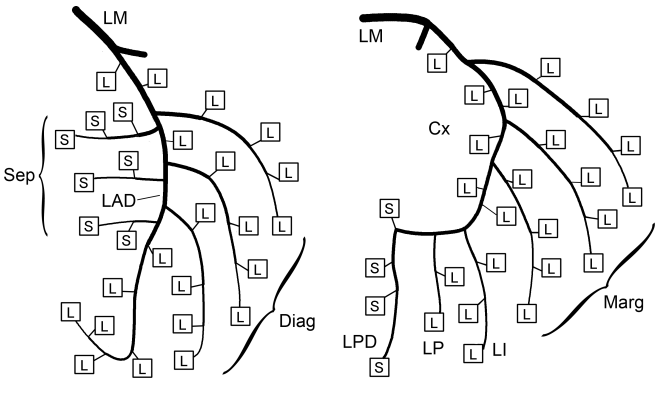

Fig. 1. Schematic of the one-dimensional conduit coronary artery model. Boxes represent instances of the 0D intramyocardial model (see Fig. 2) supplying the left ventricular free wall (L) and ventricular septum (S). Artery abbreviations: circumflex (Cx), diagonal (Diag), left anterior descending (LAD), left inferior (LI), left posterior (LP), left main (LM), left posterior descending (LPD), marginal (Marg), septal (Sep).

978-1-4577-0216-7/13/$26.00 ©2013 IEEE

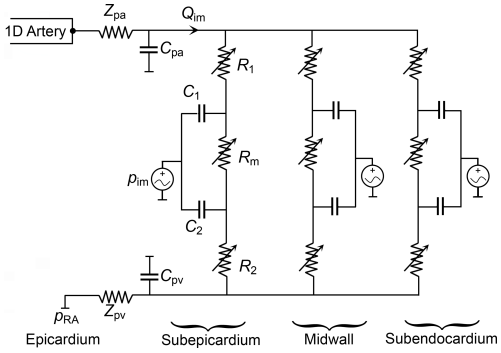

Fig. 2. Lumped parameter model of the intramyocardial circulation, see text for explanation of parameters.

via a nominal zero-area pressure of -10 mmHg [13]. External pressure ($p_{\rm ext}$) was set to zero for epicardial conduit arteries, but for septal conduit arteries that lie within the contracting ventricular septum, $p_{\rm ext}$ was set to the average of left and right ventricular cavity pressures ($p_{\rm LV}$ and $p_{\rm RV}$).

B. Lumped parameter model of coronary microvasculature

The 0D model for the coronary microvasculature (Fig. 2) was based on models described by Spaan's laboratory [2], [14]. However, instead of a single instance of the model representing the entire left coronary arterial system, in our model small 1D penetrating arteries were inserted throughout the 1D model and coupled to instances of the 0D model, each supplying a small portion of myocardium (boxes in Fig. 1). Coupling was achieved via a penetrating artery characteristic impedance and compliance ($Z_{\rm pa}$ and $C_{\rm pa}$, Fig. 2). On the venous side, a penetrating vein characteristic impedance and compliance were coupled to an assumed constant right atrial pressure ($p_{\rm RA}$ = 5 mmHg).

The microvasculature was divided into subepicardial, midwall and subendocardial layers (Fig. 2). Following [14], each layer consisted of two compartments, defined according to the compliances C_1 and C_2. Each compartment contained a resistance (R_1 and R_2), while a 'middle' resistance R_m was shared by both compartments. Subendocardial-to-subepicardial flow ratios (or left-to-right septal flow ratios) reported by Fisher et al in sheep [15] were used to set the transmural distribution of total layer resistance ($R_{\rm layer} = R_1 + R_{\rm m} + R_2$). Based on Figure 13 in [14], we assumed R_1 = $1.2R_m$ and R_2 = $0.5R_m$ and that these resistances are volume-dependent, with 75% of R_m dependent on the volume of chamber 1 and the remainder dependent on chamber 2. Based on Poiseuille's law, the chosen volume-resistance relationship was $R = R_0/V^2$ [2], given instantaneous compartment volume of

$$V(t) = V_0 + \int_0^t C\frac{dp_{\rm tm}}{dt'}dt' \qquad (3)$$

where transmural pressure ($p_{\rm tm}$) is equal to intravascular pressure minus intramyocardial pressure ($p_{\rm im}$, Fig. 2).

Intramyocardial pressure is high during systole and low during diastole, giving rise to the well-known phenomenon of systolic flow impediment. A number of mechanisms have been proposed to explain the generation and transmural distribution of $p_{\rm im}$, and are reviewed in [16]. In the current study, we utilize the finding of [17] that $p_{\rm im}$ can best be accounted for by a combination of two mechanisms. The first is cavity-induced extracellular pressure (CEP), which arises from transmission of ventricular cavity pressure into the heart wall. The second is shortening-induced intracellular pressure (SIP), which Rabbany et al. [18] hypothesized arises when myofibrils shorten and thicken to maintain a constant volume. Radial thickening of the cells would be felt by adjacent blood vessels (and pressure sensors) and thus contribute to $p_{\rm im}$ and systolic flow impediment. We therefore assumed that $p_{\rm im}$ = CEP + SIP.

As in previous modelling studies [1], [2], CEP for the LV free wall was assumed to vary linearly from cavity pressure at the endocardium to pericardial pressure (here assumed to be zero) at the epicardium. For the three transmural layers, average CEP in the subendocardium, midwall and subepicardium was therefore 5/6, 1/2 and 1/6 of $p_{\rm LV}$ respectively. For the ventricular septum, CEP was assumed to vary between $p_{\rm LV}$ and $p_{\rm RV}$ in a similar manner, and we assumed $p_{\rm RV} = 0.2p_{\rm LV}$. Unlike CEP, the same SIP was applied to all transmural layers. Consistent with measurements in [18], the SIP waveform derived in [17] was remarkably similar to the chamber elastance waveform, which attains its maximum in late systole. Thus as a first approximation, we assumed that SIP = $\alpha E_{\rm LV}$, where $E_{\rm LV}$ is left ventricular (LV) chamber elastance and α was calculated by assuming peak SIP was equal to 20% of peak $p_{\rm LV}$ [18].

For the LV and septum, C_1 and C_2 were set to 0.013 and 0.254 mL/mmHg/100g respectively, with a subendocardial-to-subepicardial ratio of 1.14 [2], [19]. In preliminary simulations, we found that accounting for the volume-dependence of compliance using the method described in [2] had a negligible effect on coronary flow waveforms, and we therefore used constant compliances. Weight-corrected quantities such as C_1 and C_2 were converted to absolute values by distributing myocardial weights according to the inverse cube of penetrating artery radii and then equally to the three transmural layers.

C. Computational Implementation

The 1D modelling techniques have been described in [12], [20]. Briefly, the non-linear 1D equations were solved using a finite element method, assuming continuity of total pressure at junctions. Standard circuit theory was used for the 0D model, with advancement in time and coupling to 1D segments using the same methods as in [20].

D. Experimental studies

Experiments were approved by the institutional ethics committee. The surgical preparation was described in [21], [22]. Briefly, nine Border-Leicester cross ewes (47.3±3.8 kg) and lambs (7-10 days old, 6.7±0.7 kg) were anaesthetised,

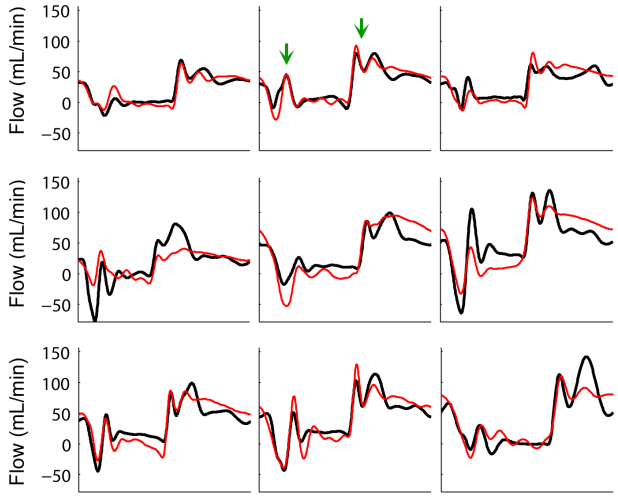

Fig. 3. Comparison of model (red) and experimental (black) flow waveforms in the proximal circumflex artery for nine adult sheep. Green arrows indicate flow transients in early systole and early diastole likely to be related to wave propagation effects.

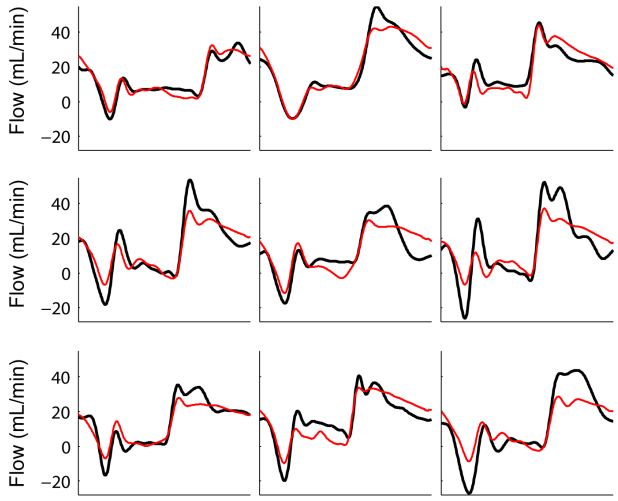

Fig. 4. Comparison of model (red) and experimental (black) flow waveforms in the proximal circumflex artery for nine newborn lambs.

intubated and ventilated to maintain normal blood gases. High fidelity pressures were measured in the ascending aorta and left ventricular cavity with 5-Fr Millar micromanometer-tipped catheters inserted via the right common carotid artery and left atrium respectively. Offset calibration of these pressures was performed with a fluid-filled catheter inserted into the aorta through a purse-string suture. High fidelity flow signals were measured in the ascending aorta and proximal circumflex coronary artery with Transonic flow probes. At the end of the study, the heart was excised and the left and right ventricular free walls and septum were weighed.

E. Validation procedure

Validation of the multi-scale coronary model was performed with minimal data fitting. In all animals, we assumed a proximal circumflex artery wave speed of 9.0 m/s, based on the reported value of 8.6 m/s in dogs [23] and the observation that, allometrically, wave speed is practically insensitive to body size [24]. Allometric scaling of 1D segment lengths and diameters was performed on the basis of measured myocardial weights and reference human myocardial weights (LV, 104 g; septum 54 g) reported in [25], using a scaling power of 0.35 [26]. Case-specific aortic pressure was prescribed at the inlet of the left main coronary artery, having applied a delay of 15 ms (sheep) and 8 ms (lambs) to account for the estimated delay between pressure generation in the myocardium and p_{LV} sensing just below the mitral valve caused by a ventricular wave speed of approximately 4 m/s [27]. Measured p_{LV} was used directly for CEP. To estimate SIP, LV cavity volume waveform was derived by integrating measured aortic flow and assuming an ejection fraction of 0.68 [28], then calculating chamber elastance as the ratio of cavity pressure and volume. Only one free parameter was considered in the validation procedure, namely total intramyocardial resistance, which was uniformly adjusted using an iterative beat-to-beat algorithm to achieve measured mean flow in the proximal circumflex artery.

III. RESULTS

Figs. 3 and 4 compare model and experimental flow waveforms for the nine sheep and nine lambs respectively. Given the lack of data fitting (aside from mean flow), the overall agreement was excellent in both groups. In particular, the levels of systolic and diastolic flow matched the in-vivo data well, although in some cases systolic flow was underestimated, suggesting overestimation of p_{im}. Importantly, flow transients in early systole and early diastole (indicated by green arrows in Fig. 3), were captured well by the model in most cases and were similar in sheep and lambs.

Fig. 5 shows the sensitivity of the model to three parameters whose estimated values were least certain. Decreasing the wave speed of all 1D segments by 22% (causing proximal circumflex wave speed to change from 9 m/s to 7 m/s) increased the magnitude of the early systolic and early diastolic flow transients; increasing wave speed suppressed these transients (Fig. 5A). If aortic pressure was applied at the model inlet without applying the delay to account for finite ventricular wave speed, a transient negative flow peak was observed in late systole that was either not present or of much lower magnitude in the experimental data; the flow waveform shape was otherwise relatively unaffected (Fig. 5B). As expected, removing SIP entirely reduced p_{im} during systole and hence increased systolic flow (via decreased systolic flow impediment); conversely, doubling SIP (peak SIP equal to 40% of CEP) led to greater systolic flow impediment (Fig. 5C).

IV. DISCUSSION AND CONCLUSIONS

This study has validated a multi-scale (0D/1D) model of the left coronary circulation using high fidelity measurements in adult sheep and newborn lambs and, to our knowledge, is the first to have modelled a left dominant coronary anatomy. Agreement between model and experimental flow waveforms in the proximal circumflex artery was excellent, despite the

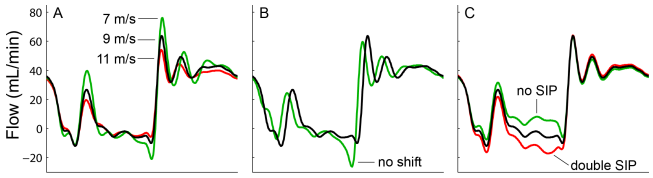

Fig. 5. (A) Sensitivity of the modelled proximal circumflex coronary artery flow waveform to wave speed (adjusted uniformly in all segments; values indicated apply to the proximal circumflex). (B) Effect of not shifting aortic pressure to account for the ventricular wave delay. (C) Effect of neglecting or doubling shortening-inducing intracellular pressure (SIP). 'Control' case (black line in each panel) is the same as the top left case in Fig. 3.

use of minimal data fitting. Since the same (scaled) conduit artery geometry and microvascular impedance model were used in all cases, differences in model waveforms between animals likely arose mainly due to differences in the waveform shape and/or amplitude of aortic and intramyocardial pressures. Overall, the model accurately captured systolic flow impediment and flow transients occurring in early systole and early diastole. These flow transients are likely to arise from wave propagation effects, since increasing or decreasing wave speed suppressed or amplified them respectively (Fig. 5A).

The lack of obvious qualitative differences between adult and newborn flow waveforms suggests that the influence of wave propagation effects may not be dependent on body size, perhaps because a higher heart frequency offsets smaller body length; however this requires further quantitative investigation. Aside from the study of coronary waves, the encouraging results presented for adults and newborns suggests that, with the use of allometric scaling, the multi-scale model may be a powerful tool for modelling coronary haemodynamics during development. In future, the multi-scale model could be easily adapted to study right dominant or other coronary anatomies, as well as right coronary arterial flow waveforms.

REFERENCES

[1] T. Arts and R. S. Reneman, "Interaction between intramyocardial pressure (IMP) and myocardial circulation," *J Biomech Eng*, vol. 107, no. 1, pp. 51–6, 1985.

[2] P. Bruinsma, T. Arts, J. Dankelman, and J. A. E. Spaan, "Model of the coronary circulation based on pressure dependence of coronary resistance and compliance," *Basic Res Cardiol*, vol. 83, no. 5, pp. 510–524, 1988.

[3] J. E. Davies, Z. I. Whinnett, D. P. Francis, K. Willson, R. A. Foale, I. S. Malik, A. D. Hughes, K. H. Parker, and J. Mayet, "Use of simultaneous pressure and velocity measurements to estimate arterial wave speed at a single site in humans," *Am J Physiol Heart Circ Physiol*, vol. 290, no. 2, pp. 878–885, 2006.

[4] P. J. Lu, C. F. J. Yang, M. Y. Wu, C. H. Hung, M. Y. Chan, and T. C. Hsu, "Wave Intensity Analysis of Para-aortic Counterpulsation," *Am J Physiol Heart Circ Physiol*, 2012.

[5] M. C. Rolandi, F. Nolte, T. P. van de Hoef, M. Remmelink, J. Baan, J. J. Piek, J. A. E. Spaan, and M. Siebes, "Coronary wave intensity during the Valsalva manoeuvre in humans reflects altered intramural vessel compression responsible for extravascular resistance," *J Physiol*, vol. 590, no. 18, pp. 4623–4635, 2012.

[6] C. Kolyva, J. A. E. Spaan, J. J. Piek, and M. Siebes, "Windkesselness of coronary arteries hampers assessment of human coronary wave speed by single-point technique," *Am J Physiol Heart Circ Physiol*, vol. 295, no. 2, pp. H482–490, 2008.

[7] J. Lee and N. P. Smith, "The Multi-Scale Modelling of Coronary Blood Flow," *Ann Biomed Eng*, 2012.

[8] J. A. Rumberger and R. M. Nerem, "A method-of-characteristics calculation of coronary blood flow," *J Fluid Mech*, vol. 82, no. 3, pp. 429–448, 1977.

[9] J. Dodge, J. T., B. G. Brown, E. L. Bolson, and H. T. Dodge, "Lumen diameter of normal human coronary arteries. Influence of age, sex, anatomic variation, and left ventricular hypertrophy or dilation," *Circulation*, vol. 86, no. 1, pp. 232–246, 1992.

[10] E. Bertho and G. Gagnon, "A Comparative Study in Three Dimension of the Blood Supply of the Normal Interventricular Septum in Human, Canine, Bovine, Porcine, Ovine and Equine Heart," *CHEST Journal*, vol. 46, no. 3, pp. 251–262, 1964.

[11] M. S. Olufsen, "Structured tree outflow condition for blood flow in larger systemic arteries," *Am J Physiol Heart Circ Physiol*, vol. 276, no. 1, pp. H257–268, 1999.

[12] J. P. Mynard and P. Nithiarasu, "A 1D arterial blood flow model incorporating ventricular pressure, aortic valve and regional coronary flow using the locally conservative Galerkin (LCG) method," *Comm Num Meth Eng*, vol. 24, no. 5, pp. 367–417, 2008.

[13] J. P. Mynard, M. R. Davidson, D. J. Penny, and J. J. Smolich, "A numerical model of neonatal pulmonary atresia with intact ventricular septum and RV-dependent coronary flow," *Int J Num Meth Biomed Eng*, vol. 26, no. 7, pp. 843–861, 2010.

[14] J. A. E. Spaan, A. J. M. Cornelissen, C. Chan, J. Dankelman, and F. C. P. Yin, "Dynamics of flow, resistance, and intramural vascular volume in canine coronary circulation," *Am J Physiol Heart Circ Physiol*, vol. 278, no. 2, pp. H383–403, 2000.

[15] D. J. Fisher, M. A. Heymann, and A. M. Rudolph, "Regional myocardial blood flow and oxygen delivery in fetal, newborn, and adult sheep," *Am J Physiol Heart Circ Physiol*, vol. 243, no. 5, pp. H729–731, 1982.

[16] N. Westerhof, C. Boer, R. R. Lamberts, and P. Sipkema, "Cross-Talk Between Cardiac Muscle and Coronary Vasculature," *Physiol Rev*, vol. 86, no. 4, pp. 1263–1308, 2006.

[17] D. Algranati, G. S. Kassab, and Y. Lanir, "Mechanisms of myocardium-coronary vessel interaction," *Am J Physiol Heart Circ Physiol*, vol. 298, no. 3, pp. H861–873, 2010.

[18] S. Y. Rabbany, J. Y. Kresh, and A. Noordergraaf, "Intramyocardial pressure: interaction of myocardial fluid pressure and fiber stress," *Am J Physiol Heart Circ Physiol*, vol. 257, no. 2, pp. H357–364, 1989.

[19] H. Weiss and M. Winbury, "Nitroglycerin and chromonar on small-vessel blood content of the ventricular walls," *Am J Physiol*, vol. 226, no. 4, pp. 838–843, 1974.

[20] J. P. Mynard, M. R. Davidson, D. J. Penny, and J. J. Smolich, "A simple, versatile valve model for use in lumped parameter and one-dimensional cardiovascular models," *Int J Num Meth Biomed Eng*, vol. 28, no. 6-7, pp. 626–641, 2012.

[21] J. J. Smolich, T. Sano, and D. J. Penny, "Blunting of pulmonary but not systemic vasodilator responses to dobutamine in newborn lambs," *Pediatr Res*, vol. 47, no. 1, pp. 107–13, 2000.

[22] D. J. Penny, J. P. Mynard, and J. J. Smolich, "Aortic wave intensity analysis of ventricular-vascular interaction during incremental dobutamine infusion in adult sheep," *Am J Physiol Heart Circ Physiol*, vol. 294, no. 1, pp. H481–489, 2008.

[23] T. Arts, R. T. Kruger, W. van Gerven, J. A. Lambregts, and R. S. Reneman, "Propagation velocity and reflection of pressure waves in the canine coronary artery," *Am J Physiol Heart Circ Physiol*, vol. 237, no. 4, pp. H469–474, 1979.

[24] B. Günther, "Allometric ratios, invariant numbers and the theory of biological similarities," *Pflügers Arch Eur J Physiol*, vol. 331, no. 4, pp. 283–293, 1972.

[25] C. H. Lorenz, E. S. Walker, V. L. Morgan, S. S. Klein, and T. P. Graham, "Normal human right and left ventricular mass, systolic function, and gender differences by cine magnetic resonance imaging," *J Cardiovasc Magn Reson*, vol. 1, no. 1, pp. 7 – 21, 1999.

[26] T. Sluysmans and S. D. Colan, "Theoretical and empirical derivation of cardiovascular allometric relationships in children," *J Appl Physiol*, vol. 99, no. 2, pp. 445–457, 2005.

[27] J. J. Wang, K. H. Parker, and J. V. Tyberg, "Left ventricular wave speed," *J Appl Physiol*, vol. 91, no. 6, pp. 2531–6, 2001.

[28] L. E. Hudsmith, S. E. Petersen, J. M. Francis, M. D. Robson, and S. Neubauer, "Normal human left and right ventricular and left atrial dimensions using steady state free precession magnetic resonance imaging," *J Cardiovasc Magn Reson*, vol. 7, no. 5, pp. 775–82, 2005.